

Scalable Autoregressive 3D Molecule Generation

Austin H. Cheng^{1,2,3}, Chong Sun⁴, Alán Aspuru-Guzik^{1,2,3,5,6,7,8,9}

¹Department of Chemistry, University of Toronto, Toronto, ON, Canada

²Department of Computer Science, University of Toronto, Toronto, ON, Canada

³Vector Institute for Artificial Intelligence, Toronto, ON, Canada

⁴Department of Chemistry and Chemical Biology, Rutgers University, Piscataway, NJ, USA

⁵Department of Materials Science & Engineering, University of Toronto, Toronto, ON, Canada

⁶Department of Chemical Engineering & Applied Chemistry, University of Toronto, Toronto, ON, Canada

⁷Senior Fellow, Canadian Institute for Advanced Research (CIFAR), Toronto, ON, Canada

⁸Acceleration Consortium, Toronto, ON, Canada

⁹NVIDIA

Generative models of 3D molecular structure play a rapidly growing role in the design and simulation of molecules. Diffusion models currently dominate the space of 3D molecule generation, while autoregressive models have trailed behind. In this work, we present QUETZAL, a simple but scalable autoregressive model that builds molecules atom-by-atom in 3D. Treating each molecule as an ordered sequence of atoms, QUETZAL combines a causal transformer that predicts the next atom’s discrete type with a smaller Diffusion MLP that models the continuous next-position distribution. Compared to existing autoregressive baselines, QUETZAL achieves substantial improvements in generation quality and is competitive with the performance of state-of-the-art diffusion models. In addition, by reducing the number of expensive forward passes through a dense transformer, QUETZAL enables significantly faster generation speed, as well as exact divergence-based likelihood computation. Finally, without any architectural changes, QUETZAL natively handles variable-size tasks like hydrogen decoration and scaffold completion. We hope that our work motivates a perspective on scalability and generality for generative modelling of 3D molecules.

1 Introduction

Generative models of 3D molecular structure are accelerating the design and simulation of molecules, with applications across chemistry, biology, and materials science (Abramson et al., 2024; Watson et al., 2023; Zeni et al., 2025). Diffusion-based approaches are the prevailing standard (Hoogetboom et al., 2022; Song et al., 2024a; Zhang et al., 2024; Joshi et al., 2025), but they typically operate on fixed-size input/output and are computationally intensive to sample from. In contrast, autoregressive models of 3D molecules have lagged behind in generation quality (Gebauer et al., 2019; Luo and Ji, 2022; Daigavane et al., 2023; Flam-Shepherd and Aspuru-Guzik, 2023; Gao et al., 2024). However, autoregressive models offer several compelling advantages: they support arbitrary-size generation, enable exact likelihood computation, and offer potentially faster generation. Moreover, molecules have a natural tokenization in terms of atoms, which aligns with the paradigm of autoregression.

This performance gap is often attributed to the assumption that diffusion models are suited for continuous spatial data, whereas autoregressive models are designed for discrete domains like text. Indeed, prior autoregressive methods for 3D structure typically *discretize* coordinates into 3D grids or tokenized .xyz files, discarding important information about spatial continuity. Recent work by Li et al. (2024a) challenges this assumption by introducing a Diffusion Loss, which jointly trains a lightweight, per-token diffusion model with an autoregressive transformer. This hybrid architecture enables autoregressive generation of continuous-valued tokens while retaining the scalability of transformers.

In this work, we adopt and extend this idea for 3D molecule generation. We propose QUETZAL, a simple yet scalable autoregressive model that generates molecules atom-by-atom, predicting each atom’s discrete type and continuous 3D position. QUETZAL combines a causal transformer with a small Diffusion MLP to

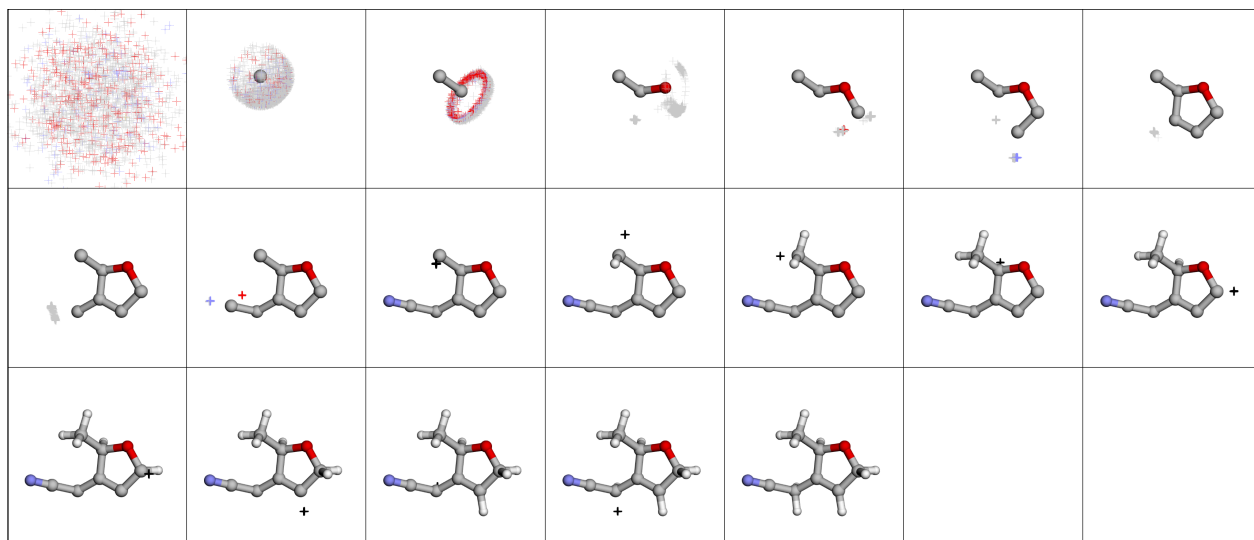


Figure 1 QUETZAL generates 3D molecules by iteratively predicting the next atom’s discrete type and continuous position. Cross marks indicate the distribution of the next atom’s type and position.

model the position of the next atom, conditioned on the current prefix structure. This simple design enables QUETZAL to scale, achieving generation quality that surpasses all autoregressive baselines and competes with state-of-the-art diffusion models, while also significantly improving generation speed. Furthermore, QUETZAL natively supports flexible generation tasks such as hydrogen decoration and scaffold completion, which are cumbersome to implement with fixed-size diffusion models.

By revisiting autoregression through the lens of modern scaling but with a continuous spatial inductive bias, QUETZAL repositions autoregressive models as a competitive and versatile approach for 3D molecule generation. Our contributions are:

- We introduce QUETZAL, an autoregressive model for 3D molecule generation that sequentially predicts the next atom’s discrete type and continuous 3D coordinates.
- We demonstrate that QUETZAL outperforms previous autoregressive approaches and competes with the performance of state-of-the-art diffusion models on QM9 and GEOM, while significantly reducing generation time.
- We show that QUETZAL enables novel capabilities over diffusion models, including exact divergence-based likelihood computation and arbitrary-size generation for hydrogen decoration and scaffold completion.

2 Related Work

3D molecular generative models. Generative models of 3D molecules have been proposed using normalizing flows (Garcia Satorras et al., 2021), diffusion models (Hoogeboom et al., 2022), flow matching (Song et al., 2024a), Bayesian flow networks (Song et al., 2024b), and latent diffusion (Xu et al., 2023; Joshi et al., 2025). Further works have enhanced generation capability by leveraging representation conditioning (Li et al., 2024b) or optimal transport (Hong et al., 2024). These approaches are often designed around equivariant architectures and typically model molecules as unordered point clouds. Other representations such as voxel grids (O Pinheiro et al., 2024) and neural fields (Kirchmeyer et al., 2025) have also been explored, which move beyond fixed-size generation.

Autoregressive 3D molecular generative models. Autoregressive models such as G-SchNet (Gebauer et al., 2019) and Symphony (Daigavane et al., 2023) discretize 3D coordinates and predict relative positions using equivariant architectures. Other models (Luo and Ji, 2022; Liu et al., 2022) predict continuous quantities using normalizing flows or mixture models, but remain tied to reference frames. Another line of work simply casts

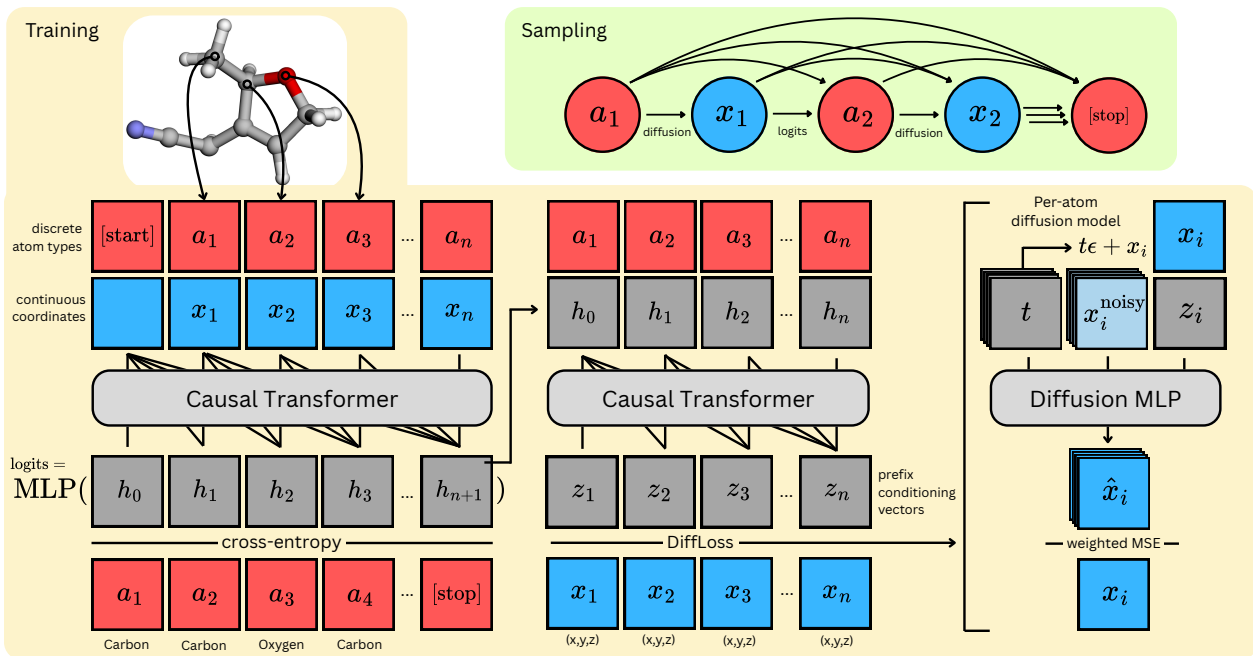


Figure 2 Architecture of QUETZAL during training and sampling. The first transformer stack causally processes each prefix of an input structure to predict logits of the next atom type. The second transformer stack incorporates information of the next atom type and causally produces conditioning vectors for the next 3D position. The prefix-conditional, per-token Diffusion MLP is trained jointly with the transformer stack using multiple timesteps. Simultaneously batching across length and time provides dense supervision signal. Sampling iteratively predicts atom type and 3D position until [stop] is predicted.

3D generative modelling as discrete language modelling of raw .xyz files (Flam-Shepherd and Aspuru-Guzik, 2023; Gruver et al., 2024; Zhulus et al., 2024; Gan et al., 2025) or using custom tokenized representations (Wang et al., 2025; Gao et al., 2024).

Autoregression over continuous-valued tokens. The most directly related work to ours is masked autoregression (MAR) (Li et al., 2024a), which introduces a Diffusion Loss for continuous-valued per-token generation in tandem with an autoregressive transformer backbone. Other approaches such as TimeGrad (Rasul et al., 2021) and Diffusion Forcing (Chen et al., 2024) apply similar prefix-conditional, per-token diffusion models for generating continuous-valued sequences. Instead of per-token diffusion, Jetformer predicts per-token Gaussian mixture parameters (Tschannen et al., 2024), and in this way trains a normalizing flow that understands text and images in data space. Trans-dimensional jump diffusion enables a diffusion model to add new dimensions during generation, which resembles autoregression (Campbell et al., 2024).

3 Method

We consider a 3D molecule $\mathcal{M} = (\mathbf{a}, \mathbf{x})$ as an *ordered* sequence of atom types $\mathbf{a} = (a_1, \dots, a_n) \in \mathbb{N}^n$ and coordinates $\mathbf{x} = (x_i, y_i, z_i)_{i=1}^n = (\mathbf{x}_1, \dots, \mathbf{x}_n) \in \mathbb{R}^{n \times 3}$, where the molecule contains n atoms. We tokenize sequences into atoms, so we refer to atoms and tokens interchangeably. We denote $\mathbf{x}_{:i} = (\mathbf{x}_1, \dots, \mathbf{x}_i)$ as the *prefix* of \mathbf{x} at sequence index i , which contains the current token and all previous tokens. We refer to $(\mathbf{a}_{:i}, \mathbf{x}_{:i})$ as the *prefix structure*. We index from 1, so $(\mathbf{a}_{:0}, \mathbf{x}_{:0})$ is null.

We define an autoregressive model of 3D molecules which iteratively predicts the next atom’s type and position $(a_{i+1}, \mathbf{x}_{i+1})$ given a prefix structure $(\mathbf{a}_{:i}, \mathbf{x}_{:i})$, as shown in Figure 1.

$$p(\mathcal{M}) = \prod_{i=0} p(a_{i+1}, \mathbf{x}_{i+1} | \mathbf{a}_{:i}, \mathbf{x}_{:i}) = \prod_{i=0} p_{\text{type}}(a_{i+1} | \mathbf{a}_{:i}, \mathbf{x}_{:i}) p_{\text{coord}}(\mathbf{x}_{i+1} | \mathbf{a}_{:i+1}, \mathbf{x}_{:i}) \quad (1)$$

The model alternates between predicting a_i and \mathbf{x}_i (i.e. sampling from p_{type} and p_{pos}) until a [stop] token is predicted, or until a maximum number of atoms is reached. The [stop] token is considered as an atom type, so p_{type} is also responsible for modelling whether to stop generation. The generative model is fully specified when we specify these two conditional distributions. The next-type distribution $p_{\text{type}}(a_{i+1}|\mathbf{a}_{:i}, \mathbf{x}_{:i})$ is a categorical distribution. This is straightforward to model using a standard GPT. First, we embed the prefix structure $(\mathbf{a}_{:i}, \mathbf{x}_{:i})$ using embeddings for the atom types, linear layers and Fourier encodings (Tancik et al., 2020) for the coordinates, and learned positional encodings for sequence ordering. The combined embeddings are then passed through a causal transformer (Vaswani, 2017):

$$\mathbf{h}_i = \text{Transformer}(\text{Emb}(\mathbf{a}_{:i}) + \text{Lin}(\mathbf{x}_{:i}) + \text{Lin}(\text{Fourier}(\mathbf{x}_{:i})) + \text{PosEmb}_{:i}). \quad (2)$$

Because attention is causally masked, the causal transformer produces prefix embeddings \mathbf{h}_i for all prefixes in the sequence in one forward pass (Figure 2). Each prefix embedding \mathbf{h}_i is then passed to a multi-layer perceptron (MLP) which predicts logits of the next atom type,

$$p(a_{i+1}|\mathbf{a}_{:i}, \mathbf{x}_{:i}) = p(a_{i+1}|\mathbf{h}_i) = \text{softmax}(\text{MLP}(\mathbf{h}_i)), \quad (3)$$

which are supervised by cross-entropy loss against the ground truth next atom types.

What remains is to model the next 3D position distribution $p_{\text{pos}}(\mathbf{x}_{i+1}|\mathbf{a}_{:i+1}, \mathbf{x}_{:i})$. Here, instead of discretizing \mathbf{x} , we use the Diffusion Loss proposed by Li et al. (2024a) to model the continuous distribution p_{pos} . In other words, we model p_{pos} as a diffusion model that generates a single 3D position, conditioned on a prefix structure and next atom type. We first combine the prefix embeddings $\mathbf{h}_{:i}$ with the next atom type \mathbf{a}_{i+1} and pass through a second transformer to obtain the single-atom conditioning vector \mathbf{z}_i , which conditions the diffusion model:

$$p_{\text{pos}}(\mathbf{x}_{i+1}|\mathbf{a}_{:i+1}, \mathbf{x}_{:i}) = p(\mathbf{x}_{i+1}|\mathbf{z}_{i+1}), \text{ where } \mathbf{z}_{i+1} = \text{Transformer}(\text{Emb}(\mathbf{a}_{:i+1}) + \mathbf{h}_{:i}). \quad (4)$$

This structure forces the model to commit to a discrete atom type before predicting its continuous position, which we find is beneficial for learning.

We now introduce diffusion models, and temporarily drop the subscripts and the conditioning vector. Our approach closely follows Karras et al. (2022). Diffusion models learn to sample from a continuous distribution defined by a dataset $p_{\text{data}}(\mathbf{x})$. We can corrupt data by taking every data example and adding i.i.d. Gaussian noise with standard deviation that scales linearly with time t . This defines a time-dependent probability density $p_t(\mathbf{x})$ described by convolving the data distribution with a Gaussian whose standard deviation is linearly increasing in time, $p_t(\mathbf{x}) = p_{\text{data}}(\mathbf{x}) \otimes \mathcal{N}(\mathbf{0}, t^2 \mathbf{I})$. At small times, p_0 approximates the data distribution, whereas for large time T , p_T is well approximated as a large Gaussian $\mathcal{N}(\mathbf{0}, T^2 \mathbf{I})$, which can be sampled without knowing p_{data} . Then, a remarkable result is that samples $\mathbf{x}_t \sim p_t(\mathbf{x}_t)$ can be generated by drawing samples $\mathbf{x}_T \sim p_T(\mathbf{x}_T)$ and evolving them backwards from time T to t under the probability flow ODE (Song et al., 2020a; Karras et al., 2022),

$$d\mathbf{x} = -t\nabla_{\mathbf{x}} \log p_t(\mathbf{x})dt, \quad (5)$$

which can be done as long as we know the time-dependent score function $\nabla_{\mathbf{x}} \log p_t(\mathbf{x})$. This score function is learned by a neural network $\mathbf{s}_{\theta}(t, \mathbf{x})$ with parameters θ , which is trained by minimizing the denoising score matching objective (Vincent, 2011) for every t :

$$\mathbb{E}_{\mathbf{x} \sim p_{\text{data}}, \varepsilon \sim \mathcal{N}(0, I)} \|\mathbf{s}_{\theta}(t, \mathbf{x} + t\varepsilon) + \frac{\varepsilon}{t}\|^2. \quad (6)$$

By Tweedie’s formula (Efron, 2011),

$$D(t, \mathbf{y}) = \mathbf{y} + t^2 \nabla_{\mathbf{y}} \log p_t(\mathbf{y}), \quad (7)$$

this objective can be rewritten as learning an optimal denoiser $D_{\theta}(t, \mathbf{x}^{\text{noisy}})$ that aims to predict the original data \mathbf{x} from the corrupted data $\mathbf{x}^{\text{noisy}} = \mathbf{x} + t\varepsilon$,

$$\mathbb{E}_{\mathbf{x} \sim p_{\text{data}}, \varepsilon \sim \mathcal{N}(0, I)} \|D_{\theta}(t, \mathbf{x} + t\varepsilon) - \mathbf{x}\|^2. \quad (8)$$

A diffusion model can be easily extended to conditional distributions by simply providing a conditioning vector \mathbf{z} as an extra input to the network. We now define the next-position distribution as a conditional diffusion

model whose target distribution is $p_{\text{pos}}(\mathbf{x}_i|\mathbf{z}_i)$, giving the following objective for learning the next-position distribution:

$$\mathbb{E}_{\mathbf{x}_i \sim p_{\text{pos}}, \boldsymbol{\varepsilon} \sim \mathcal{N}(0, I)} \|D_\theta(t, \mathbf{x}_i + t\boldsymbol{\varepsilon}, \mathbf{z}_i) - \mathbf{x}_i\|^2, \quad (9)$$

which is a restatement of DiffLoss (Li et al., 2024a). We then predict $\hat{\mathbf{x}}_i = D_\theta(t, \mathbf{x}_i^{\text{noisy}}, \mathbf{z}_i)$ using a Diffusion MLP (DiffMLP) with adaptive layer normalization (Perez et al., 2017; Peebles and Xie, 2022), zero-initialization (Peebles and Xie, 2022), and residual connections (He et al., 2015):

$$\hat{\mathbf{x}}_i = \text{DiffMLP} \left(\text{Fourier}(t) + \text{Lin}(\mathbf{x}_i^{\text{noisy}}) + \text{Lin}(\text{Fourier}(\mathbf{x}_i^{\text{noisy}})) + \text{Lin}(\mathbf{z}_i) \right). \quad (10)$$

During training, once the conditioning vector \mathbf{z}_i has been constructed, we independently sample 4 timesteps t to expand the batch size used for training the DiffMLP. Once the denoiser is trained, one now has access to the score through Equation (7), and can sample p_{pos} by drawing random noise and integrating Equation (5) from time $t = T$ to $t = 0$, using N_{diff} discretized timesteps. See Appendix A for further details on sampling, preconditioning the neural network, and timestep-weighting during training.

Molecules have translation, rotation, and permutation symmetries. To avoid overfitting to particular orientations, we apply simple data augmentation with random rotations and random translations of up to 3\AA during training. We first center all training examples so that their center-of-mass is at the origin. We treat molecules as ordered sequences of atoms, and we inherit the ordering of atoms as listed in the .xyz file. This ordering is likely to have originated from how the original 3D structure was initialized from SMILES, or drawn by hand, which importantly provides a localized ordering of atoms.

The now-defined architecture has several characteristics to note: It relies on standard deep learning components, such as transformers and MLPs, which have optimized hardware implementations such as FlashAttention (Dao, 2023) and optimized kernels by torch.compile (Ansel et al., 2024). It provides dense training supervision on every atom type and position, owing to the ability of causal transformers to efficiently batch sequences across length, while simultaneously allowing batching across multiple timesteps for training the DiffMLP. It separates the concerns of generative modelling into modelling quadratic-scaling atom *interdependence* with transformers, and modelling *individual* next-type/position distributions using MLPs. The generation cost for QUETZAL is $O(n)$ transformer forward passes (one per atom) and $O(nN_{\text{diff}})$ coordinate updates using a MLP. In contrast, all-atom diffusion would require N_{diff} passes through a transformer or similarly expensive architecture. This architectural distinction enables significantly faster sampling for QUETZAL, especially on small molecules. QUETZAL operates in data-space and does not require learning a separate tokenizer (Liu et al., 2024). Thus, QUETZAL accepts any 3D structure as input and generates arbitrary-size output, which enables flexible use for downstream tasks such as hydrogen decoration and scaffold completion.

The causal transformer blocks are identical to GPT-2 (Radford et al., 2019), using the implementation of nanoGPT (Karpathy, 2025), except we apply qk-layernorm along the head dimension for training stability (Chowdhery et al., 2023; Wortsman et al., 2023), and we do not apply a final LayerNorm before output projection. Biases are also disabled in transformer blocks. For an architecture with L transformer blocks, the first $L/2$ blocks are used for predicting \mathbf{h}_i , while the second $L/2$ blocks are used for predicting \mathbf{z}_i . To reduce padding, we use sequence packing (Krell et al., 2021).

3.1 Likelihood

In diffusion models, the change-of-variables formula (Chen et al., 2018) can be used to compute the log-likelihood $\log p_0(x_0)$ for a given data point x_0 :

$$\log p_0(x_0) = \log p_T(x_T) + \int_0^T \nabla \cdot \mathbf{s}_\theta(t, x_t) dt \quad (11)$$

Computing $\nabla \cdot \mathbf{s}_\theta(t, x_t)$, which is the divergence (trace-Jacobian) of the score function, requires computing d vector-Jacobian products, where d is the dimensionality of the data. In pure diffusion models, this is expensive because d is large (e.g. $d = 3n \approx 132$ for GEOM with an average of 44 atoms). Therefore, most approaches resort to estimating log-likelihood via the ELBO or by approximating the divergence term using the Hutchinson trace estimator (Hutchinson, 1989). However, since the DiffMLP operates on 3-dimensional data, it is tractable to compute exact log-likelihood for each atom position by explicitly computing the full 3×3 Jacobian.

Table 1 Sample quality of unconditionally generated molecules from QM9 by validity and uniqueness when generating 10,000 examples. Results for QUETZAL are means and standard deviations across 3 evaluation runs. QUETZAL uses $N_{\text{diff}} = 60$. Results on xyz2mol taken from (Gao et al., 2024), other results from respective works or *from our own evaluation. Higher is better, except for NLL.

	atom stable	mol stable	lookup valid	lookup valid×uniq	xyz2mol valid	xyz2mol valid×uniq	NLL (↓)
QM9	99.36	95.30	97.67	97.63	99.99	99.90	
EDM	98.7	82.0	91.9	90.7	86.7	86.0	-110.70
GeoLDM	98.9	89.4	93.8	92.7	91.3	90.3	-
SymDiff	98.9	89.7	96.4	94.1	92.8*	91.4*	-133.79
G-SchNet	95.7	68.1	85.5	80.3	75.0	72.5	-
Symphony	90.8	43.9	68.1	66.5	83.5	81.8	-
Mol-StrucTok	98.5	88.3	98.0	83.4	96.7	82.5	-
QUETZAL	98.7 ±0.0	90.4 ±0.4	95.7 ±0.2	90.2 ±0.2	98.6 ±0.1	94.0 ±0.3	-97.03

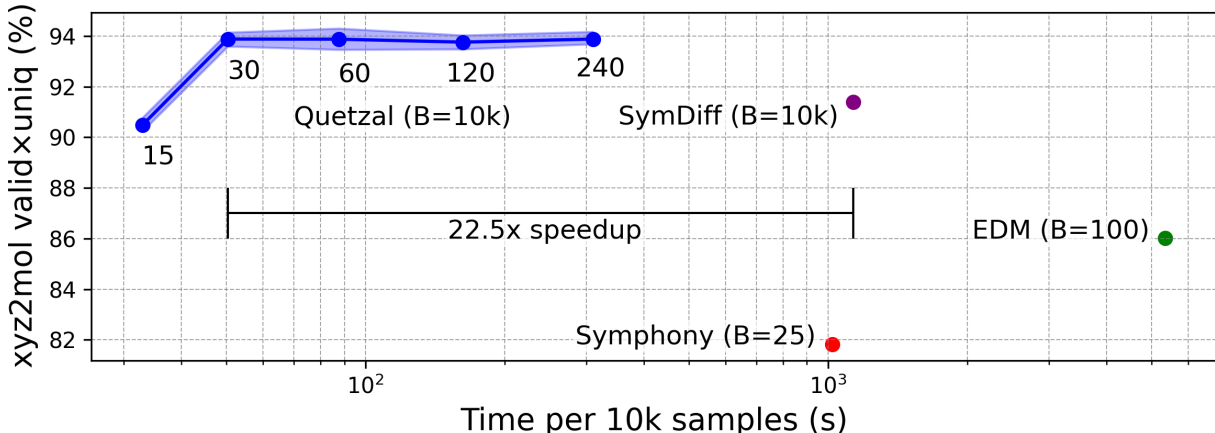


Figure 3 xyz2mol validity×uniqueness of 10k samples as a function of generation speed for QM9. B is the batch size used for generation. We show the largest batch size that fits on a single A100 40 GB GPU. For QUETZAL, the text annotation is the number of diffusion steps used per atom. Error bars show min/max over 5 evaluations. See Appendix Figure 7 for generation speed vs batch size.

4 Experiments

4.1 Molecular generation

We train QUETZAL on unconditional 3D molecular generation from the QM9 (Ramakrishnan et al., 2014) and GEOM-DRUGS (Axelrod and Gomez-Bombarelli, 2022) datasets (abbreviated as GEOM). We follow the train/val/test splits of Hoogeboom et al. (2022), as well as their evaluation protocol of generating 10,000 molecules and assessing atom stability, molecule stability, and validity and uniqueness via bond lookup tables. We also assess validity and uniqueness via xyz2mol as introduced by Daigavane et al. (2023). Finally, we assess negative log-likelihood (NLL) of the test set according to each model. We implement QUETZAL using a 12-layer transformer (12 attention heads, hidden size 768, 86M parameters) and a 6-layer DiffMLP (hidden size 1536, 79M parameters), resulting in 165M total parameters. More details on metrics, evaluation, generated samples, and ablation studies are in Appendix B.

Baselines. We compare to equivariant diffusion models EDM (Hoogeboom et al., 2022), GeoLDM (Xu et al., 2023), and SymDiff (Zhang et al., 2024). EDM and GeoLDM use equivariant graph neural networks (EGNNs)

Table 2 Sample quality of unconditionally generated molecules from GEOM by validity and uniqueness. QUETZAL uses $N_{\text{diff}} = 120$ for generation and $N_{\text{diff}} = 60$ for NLL. *We assume uniqueness is 100%.

	atom stable	lookup valid	lookup valid \times uniq	NLL (\downarrow)
GEOM	86.5	99.9	69.5	
EDM	81.3	92.6	92.6*	-137.1
GeoLDM	84.4	99.3	99.3*	-
GCDM	89.0	95.5	95.5*	-234.3
SymDiff	86.2	99.3	99.3*	-301.21
QUETZAL	86.7 \pm 0.0	95.6 \pm 0.1	95.3 \pm 0.2	-313.63

(Satorras et al., 2021), whereas SymDiff uses a permutation-equivariant diffusion transformer that scalably incorporates rotation equivariance via stochastic symmetrization. We also compare to autoregressive models G-SchNet (Gebauer et al., 2019) and Symphony (Daigavane et al., 2023), which rely on equivariant, relative predictions of the next atom position, as well as Mol-StrucTok (Gao et al., 2024), which tokenizes 3D structures into an SE(3)-invariant line notation for language modeling. All autoregressive baselines discretize 3D space.

4.2 QM9 generation results

Validity and uniqueness. QUETZAL achieves strong sample quality on QM9, outperforming prior autoregressive methods in both xyz2mol and lookup table metrics (Table 1), and surpassing pure diffusion models in xyz2mol metrics. Interestingly, QUETZAL exhibits signs of overfitting as evidenced by high validity but reduced validity \times uniqueness. QUETZAL also obtains a poor estimate of test-set log-likelihood, despite generating high-quality samples. These observations may stem from QUETZAL overfitting to the fixed atom orderings seen during training.

Generation efficiency. QUETZAL generates molecules significantly faster than all baselines, despite having the most parameters. Figure 3 shows the tradeoff between sample quality and generation time on a single A100 40GB GPU, where each model is run with the largest batch size that fits in memory. At $N_{\text{diff}} = 30$, QUETZAL achieves a 22.5 \times speedup over SymDiff while obtaining better xyz2mol validity \times uniqueness. Although recent samplers (Song et al., 2020b; Lu et al., 2022; Karras et al., 2022) can reduce inference steps for diffusion models, matching QUETZAL’s speed would require reducing SymDiff’s 1000 steps to fewer than 44 — while preserving quality. Importantly, QUETZAL could also benefit from such sampler improvements. In Appendix Figure 7, we show that generation throughput also scales well with batch size.

The speed can be attributed to several factors: (1) Whereas pure diffusion models require a dense pass through the transformer on every timestep, QUETZAL only calls the transformer once per new atom, and instead relies on cheaper passes through the MLP for diffusion. (2) The number of diffusion steps is also largely reduced by using the Heun sampler and geometrically-spaced timesteps proposed by Karras et al. (2022). (3) Forward passes are cheaper because the optimized performance of FlashAttention (Dao, 2023) is much faster than expensive message-passing steps of EGNN (Satorras et al., 2021) or tensor products for Symphony.

4.3 GEOM generation

QUETZAL is, to our knowledge, the first autoregressive model demonstrated on the large and diverse GEOM dataset. We compare to diffusion-based baselines including GCDM (Morehead and Cheng, 2024). QUETZAL again achieves generation quality approaching that of diffusion models (Table 2), but with much faster sampling: QUETZAL ($N_{\text{diff}} = 120$) requires 11.9 minutes for 10k samples, whereas EDM requires 1,533 minutes (128 \times speedup) and GCDM requires 683 minutes (57 \times speedup). Interestingly, QUETZAL achieves state-of-the-art NLL on GEOM, despite underperforming on QM9. We hypothesize that this is due to random splitting of GEOM: The dataset includes up to 30 conformers per molecule, so most molecules in the test set have conformers that are seen in the training set. This also explains why lookup validity \times uniqueness of the original training set is low. We show uncurated samples in Appendix Figure 10.

Table 3 Method performance on adding hydrogens onto bare molecules from the test set of QM9. All results are from our own evaluation. *Checkpoint appears to be undertrained, see [Appendix B.3](#).

Method	Correct	% < RMSD Å		
	Num H	0.5	0.1	0.05
Olex2	62.7	57.1	7.8	0.1
OpenBabel+Hydride	88.4	79.0	42.9	12.7
Symphony*	46.9	43.6	34.9	23.8
QUETZAL	99.8	99.5	94.1	90.4

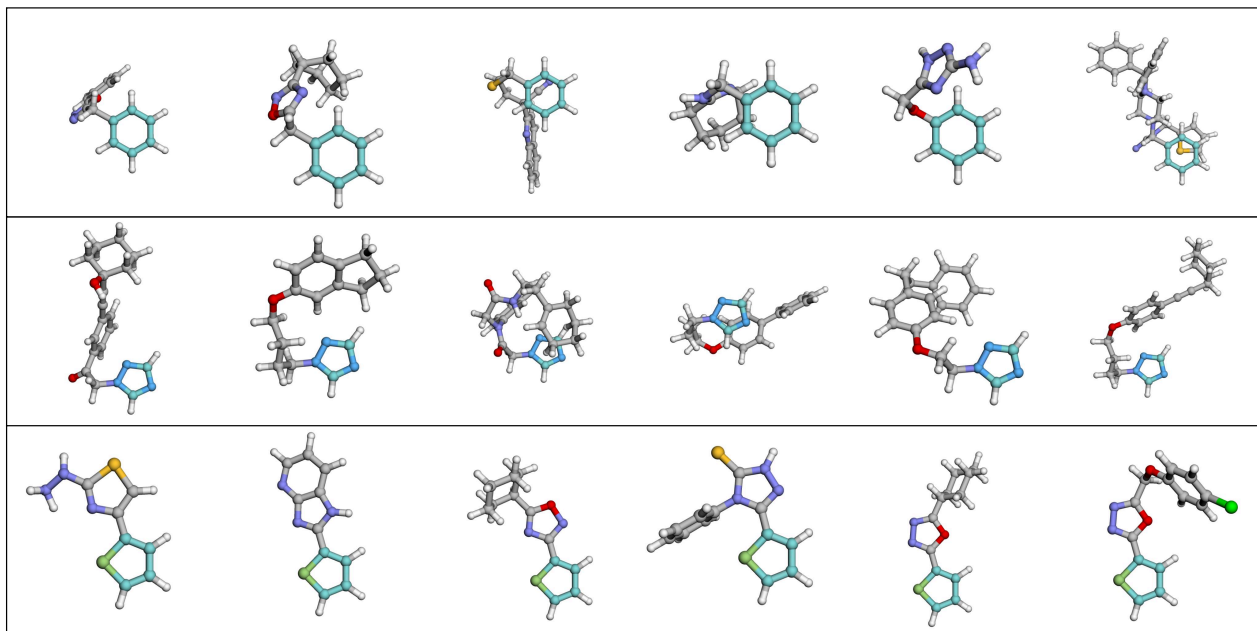


Figure 4 Selected examples of scaffold completion for benzene, 1,2,4-triazole, and thiophene. Generation uses $N_{\text{diff}} = 120$.

4.4 Hydrogen decoration

Because QUETZAL generates atoms sequentially, with hydrogens typically last, it can be applied with no additional training to decorate 3D structures with missing hydrogens. This task is useful for adding hydrogens to 3D structures from X-ray crystallography, which often lack resolved hydrogens due to low electron density (Müller, 2009). Typically, this task is performed with specialized cheminformatics software. It is unclear how to apply pure diffusion models to the task of hydrogen decoration, as they require specifying a fixed size. Therefore, we compare to tools such as the crystallography toolbox Olex2 (Dolomanov et al., 2009), and OpenBabel + Hydride (O’Boyle et al., 2011; Kunzmann et al., 2022), which first infers bonds then adds hydrogens in 3D. We also compare to Symphony, an autoregressive model trained on QM9. We test this task by stripping hydrogens from the test set of QM9, and evaluate the accuracy in adding hydrogens back.

As metrics, we check whether each method adds the correct number of hydrogens. If the number of hydrogens is correct, we calculate the root-mean-squared deviation (RMSD) for just the hydrogen atoms, and check whether it satisfies thresholds of 0.5, 0.1, and 0.05 Å. Because hydrogens can be added in any order, we first assign permutations between predicted and ground truth by solving a linear assignment problem (Hungarian algorithm) on Euclidean distances. Results are in [Table 3](#).

QUETZAL predicts hydrogens with high accuracy. However, QUETZAL’s hydrogen predictions are sensitive to atom ordering. QUETZAL is able to solve this task because in QM9, hydrogens appear last in the .xyz files. If the bare molecule without hydrogens is reordered, QUETZAL’s performance degrades significantly, as the prefix becomes out-of-distribution. Additional results are in [Appendix B.3](#).

4.5 Scaffold completion

Scaffold completion is naturally suited to autoregressive generation, since the prefix structure is held fixed. We demonstrate completions for benzene, 1,2,4-triazole, and thiophene scaffolds in [Figure 4](#). These are qualitative results; we defer quantitative evaluation and comparison ([Xie et al., 2024](#)) to future work. We note that, like hydrogen decoration, scaffold completion is sensitive to the initial scaffold configuration in terms of its atom ordering, center of mass, and orientation. However, this can be useful to steer how the scaffold is completed.

5 Discussion

Our architecture is simple: it does not require a separate tokenizer or autoencoder, does not model bonds explicitly, does not predict a focal atom or relative coordinates, and does not architecturally consider permutation, translation, or rotation symmetries. Instead, we rely on a standard transformer backbone equipped with Diffusion Loss, a simple method for autoregressive generation of per-token continuous coordinates ([Li et al., 2024a](#)). In doing so, we create a model that is simple to implement, trainable at scale, and fast to sample from.

Despite these advantages, the model has limitations. It is not permutation-invariant. Removing positional encodings does not confer permutation symmetry, as the generation order still induces a learned ordering ([Haviv et al., 2022](#); [Kazemnejad et al., 2024](#)). This dependency on generation order also constrains generalization—e.g., the model performs poorly under random atom orderings and cannot generalize to molecules with more atoms than seen during training. In ablations, we show that randomly permuting the atom ordering leads to poor performance ([Appendix B.2](#)), similar to how training autoregressive Sudoku solvers is highly dependent on generation order ([Shah et al., 2024](#)). Therefore, we need to know the best order in which to generate atoms. Additionally, like other autoregressive models, our method is susceptible to error accumulation ([LeCun, 2023](#)) or failures in teacher-forcing ([Bachmann and Nagarajan, 2024](#)).

Future work may explore training and decoding strategies that reduce dependence on or infer atom generation order, such as masked diffusion ([Kim et al., 2025](#)). In addition, future work can also exploit the fact that autoregressive models accept *arbitrary-size input* and generate *arbitrary-size output*, which can provide extremely flexible conditioning, especially in the context of text ([Gruver et al., 2024](#)). Autoregression could also allow the model to reason for many continuous-valued tokens using chain-of-thought ([Wei et al., 2022](#); [Hao et al., 2024](#)). Finally, tractable exact likelihood computation enables importance sampling for Boltzmann generators ([Noé et al., 2019](#); [Klein et al., 2023](#); [Klein and Noé, 2024](#); [Tan et al., 2025](#)), and could unlock new strategies for finetuning models on reward functions.

This work advances molecular generative modeling, with potential to accelerate molecular simulation and discovery. These capabilities can benefit drug discovery, materials design, and the development of sustainable technologies—areas with direct impact on public health, energy, and environmental sustainability. At the same time, we acknowledge that these capabilities could advance the discovery of (bio)chemical weapons ([Urbina et al., 2022](#)). Nevertheless, the effective use or misuse of such technologies would require significant wet-lab resources and expertise.

6 Acknowledgements

A.H.C. thanks Marta Skreta and Lazar Atanackovic for helpful discussions. This research was enabled in part by computational resources provided by the Digital Research Alliance of Canada (<https://alliancecan.ca>) and the Acceleration Consortium (<https://acceleration.utoronto.ca>). A.H.C. acknowledges the generous support of the Canada 150 Research Chairs program through A.A.-G. A.A.-G. thanks Anders G. Frøseth for his generous support, and acknowledges the generous support of Natural Resources Canada and the Canada 150 Research Chairs program. This research is part of the University of Toronto’s Acceleration Consortium, which receives funding from the Canada First Research Excellence Fund (CFREF) via CFREF-2022-00042.

We acknowledge the Python community ([Van Rossum et al., 1995](#); [Oliphant, 2007](#)) for developing the core set of tools that enabled this work, including PyTorch ([Paszke et al., 2019](#)), PyTorch Lightning ([Falcon and The PyTorch Lightning team, 2019](#)), RDKit ([Landrum et al., 2023](#)), py3Dmol ([Rego and Koes, 2015](#)), Jupyter

(Kluyver et al., 2016), Matplotlib (Hunter, 2007), seaborn (Waskom, 2021), NumPy (Harris et al., 2020), SciPy (Virtanen et al., 2020), and pandas (The pandas development team).

References

- Josh Abramson, Jonas Adler, Jack Dunger, Richard Evans, Tim Green, Alexander Pritzel, Olaf Ronneberger, Lindsay Willmore, Andrew J Ballard, Joshua Bambrick, et al. Accurate structure prediction of biomolecular interactions with alphafold 3. *Nature*, pages 1–3, 2024.
- Joseph L Watson, David Juergens, Nathaniel R Bennett, Brian L Trippe, Jason Yim, Helen E Eisenach, Woody Ahern, Andrew J Borst, Robert J Ragotte, Lukas F Milles, et al. De novo design of protein structure and function with rfdiffusion. *Nature*, 620(7976):1089–1100, 2023.
- Claudio Zeni, Robert Pinsler, Daniel Zügner, Andrew Fowler, Matthew Horton, Xiang Fu, Zilong Wang, Aliaksandra Shysheya, Jonathan Crabbé, Shoko Ueda, et al. A generative model for inorganic materials design. *Nature*, pages 1–3, 2025.
- Emiel Hoogeboom, Victor Garcia Satorras, Clément Vignac, and Max Welling. Equivariant diffusion for molecule generation in 3d. In *International conference on machine learning*, pages 8867–8887. PMLR, 2022.
- Yuxuan Song, Jingjing Gong, Minkai Xu, Ziyao Cao, Yanyan Lan, Stefano Ermon, Hao Zhou, and Wei-Ying Ma. Equivariant flow matching with hybrid probability transport for 3d molecule generation. *Advances in Neural Information Processing Systems*, 36, 2024a.
- Leo Zhang, Kianoosh Ashouritaklimi, Yee Whye Teh, and Rob Cornish. Symdiff: Equivariant diffusion via stochastic symmetrisation. *arXiv preprint arXiv:2410.06262*, 2024.
- Chaitanya K Joshi, Xiang Fu, Yi-Lun Liao, Vahe Gharakhanyan, Benjamin Kurt Miller, Anuroop Sriram, and Zachary W Ulissi. All-atom diffusion transformers: Unified generative modelling of molecules and materials. *arXiv preprint arXiv:2503.03965*, 2025.
- Niklas Gebauer, Michael Gastegger, and Kristof Schütt. Symmetry-adapted generation of 3d point sets for the targeted discovery of molecules. In H. Wallach, H. Larochelle, A. Beygelzimer, F. d'Alché-Buc, E. Fox, and R. Garnett, editors, *Advances in Neural Information Processing Systems*, volume 32. Curran Associates, Inc., 2019. URL https://proceedings.neurips.cc/paper_files/paper/2019/file/a4d8e2a7e0d0c102339f97716d2fdfb6-Paper.pdf.
- Youzhi Luo and Shuiwang Ji. An autoregressive flow model for 3d molecular geometry generation from scratch. In *International conference on learning representations (ICLR)*, 2022.
- Ameya Daigavane, Song Kim, Mario Geiger, and Tess Smidt. Symphony: Symmetry-equivariant point-centered spherical harmonics for molecule generation. *arXiv preprint arXiv:2311.16199*, 2023.
- Daniel Flam-Shepherd and Alán Aspuru-Guzik. Language models can generate molecules, materials, and protein binding sites directly in three dimensions as xyz, cif, and pdb files. *arXiv preprint arXiv:2305.05708*, 2023.
- Kaiyuan Gao, Yusong Wang, Haoxiang Guan, Zun Wang, Qizhi Pei, John E Hopcroft, Kun He, and Lijun Wu. Tokenizing 3d molecule structure with quantized spherical coordinates. *arXiv preprint arXiv:2412.01564*, 2024.
- Tianhong Li, Yonglong Tian, He Li, Mingyang Deng, and Kaiming He. Autoregressive image generation without vector quantization. *arXiv preprint arXiv:2406.11838*, 2024a.
- Victor Garcia Satorras, Emiel Hoogeboom, Fabian Fuchs, Ingmar Posner, and Max Welling. E (n) equivariant normalizing flows. *Advances in Neural Information Processing Systems*, 34:4181–4192, 2021.
- Yuxuan Song, Jingjing Gong, Yanru Qu, Hao Zhou, Mingyue Zheng, Jingjing Liu, and Wei-Ying Ma. Unified generative modeling of 3d molecules via bayesian flow networks. *arXiv preprint arXiv:2403.15441*, 2024b.
- Minkai Xu, Alexander S Powers, Ron O Dror, Stefano Ermon, and Jure Leskovec. Geometric latent diffusion models for 3d molecule generation. In *International Conference on Machine Learning*, pages 38592–38610. PMLR, 2023.
- Zian Li, Cai Zhou, Xiyuan Wang, Xingang Peng, and Muhan Zhang. Geometric representation condition improves equivariant molecule generation. *arXiv preprint arXiv:2410.03655*, 2024b.
- Haokai Hong, Wanyu Lin, and Kay Chen Tan. Fast 3d molecule generation via unified geometric optimal transport. *arXiv preprint arXiv:2405.15252*, 2024.

- Pedro O O Pinheiro, Joshua Rackers, Joseph Kleinhenz, Michael Maser, Omar Mahmood, Andrew Watkins, Stephen Ra, Vishnu Sresht, and Saeed Saremi. 3d molecule generation by denoising voxel grids. *Advances in Neural Information Processing Systems*, 36, 2024.
- Matthieu Kirchmeyer, Pedro O Pinheiro, and Saeed Saremi. Score-based 3d molecule generation with neural fields. *arXiv preprint arXiv:2501.08508*, 2025.
- Meng Liu, Youzhi Luo, Kanji Uchino, Koji Maruhashi, and Shuiwang Ji. Generating 3D molecules for target protein binding. In Kamalika Chaudhuri, Stefanie Jegelka, Le Song, Csaba Szepesvari, Gang Niu, and Sivan Sabato, editors, *Proceedings of the 39th International Conference on Machine Learning*, volume 162 of *Proceedings of Machine Learning Research*, pages 13912–13924. PMLR, 17–23 Jul 2022. URL <https://proceedings.mlr.press/v162/liu22m.html>.
- Nate Gruver, Anuroop Sriram, Andrea Madotto, Andrew Gordon Wilson, C Lawrence Zitnick, and Zachary Ulissi. Fine-tuned language models generate stable inorganic materials as text. *arXiv preprint arXiv:2402.04379*, 2024.
- Artem Zholus, Maksim Kuznetsov, Roman Schutski, Rim Shayakhmetov, Daniil Polykovskiy, Sarath Chandar, and Alex Zhavoronkov. Bindgpt: A scalable framework for 3d molecular design via language modeling and reinforcement learning. *arXiv preprint arXiv:2406.03686*, 2024.
- Jingru Gan, Peichen Zhong, Yuanqi Du, Yanqiao Zhu, Chenru Duan, Haorui Wang, Carla P Gomes, Kristin A Persson, Daniel Schwalbe-Koda, and Wei Wang. Large language models are innate crystal structure generators. *arXiv preprint arXiv:2502.20933*, 2025.
- Jike Wang, Hao Luo, Rui Qin, Mingyang Wang, Xiaozhe Wan, Meijing Fang, Odin Zhang, Qiaolin Gou, Qun Su, Chao Shen, et al. 3dsmiles-gpt: 3d molecular pocket-based generation with token-only large language model. *Chemical Science*, 16(2):637–648, 2025.
- Kashif Rasul, Calvin Seward, Ingmar Schuster, and Roland Vollgraf. Autoregressive denoising diffusion models for multivariate probabilistic time series forecasting. In *International conference on machine learning*, pages 8857–8868. PMLR, 2021.
- Boyuan Chen, Diego Marti Monso, Yilun Du, Max Simchowitz, Russ Tedrake, and Vincent Sitzmann. Diffusion forcing: Next-token prediction meets full-sequence diffusion. *arXiv preprint arXiv:2407.01392*, 2024.
- Michael Tschannen, André Susano Pinto, and Alexander Kolesnikov. Jetformer: An autoregressive generative model of raw images and text. *arXiv preprint arXiv:2411.19722*, 2024.
- Andrew Campbell, William Harvey, Christian Weilbach, Valentin De Bortoli, Thomas Rainforth, and Arnaud Doucet. Trans-dimensional generative modeling via jump diffusion models. *Advances in Neural Information Processing Systems*, 36, 2024.
- Matthew Tancik, Pratul Srinivasan, Ben Mildenhall, Sara Fridovich-Keil, Nithin Raghavan, Utkarsh Singhal, Ravi Ramamoorthi, Jonathan Barron, and Ren Ng. Fourier features let networks learn high frequency functions in low dimensional domains. *Advances in neural information processing systems*, 33:7537–7547, 2020.
- A Vaswani. Attention is all you need. *Advances in Neural Information Processing Systems*, 2017.
- Tero Karras, Miika Aittala, Timo Aila, and Samuli Laine. Elucidating the design space of diffusion-based generative models. *Advances in neural information processing systems*, 35:26565–26577, 2022.
- Yang Song, Jascha Sohl-Dickstein, Diederik P Kingma, Abhishek Kumar, Stefano Ermon, and Ben Poole. Score-based generative modeling through stochastic differential equations. *arXiv preprint arXiv:2011.13456*, 2020a.
- Pascal Vincent. A connection between score matching and denoising autoencoders. *Neural computation*, 23(7):1661–1674, 2011.
- Bradley Efron. Tweedie’s formula and selection bias. *Journal of the American Statistical Association*, 106(496):1602–1614, 2011.
- E Perez, F Strub, H De Vries, V Dumoulin, and A Courville. Film: Visual reasoning with a general conditioning layer. arxiv. *arXiv preprint arXiv:1709.07871*, 2017.
- William S Peebles and Saining Xie. Scalable diffusion models with transformers. 2023 ieee. In *CVF International Conference on Computer Vision (ICCV)*, volume 4172, 2022.
- Kaiming He, Xiangyu Zhang, Shaoqing Ren, and Jian Sun. Deep residual learning for image recognition. arxiv e-prints. *arXiv preprint arXiv:1512.03385*, 10, 2015.

- Tri Dao. Flashattention-2: Faster attention with better parallelism and work partitioning. *arXiv preprint arXiv:2307.08691*, 2023.
- Jason Ansel, Edward Yang, Horace He, Natalia Gimelshein, Animesh Jain, Michael Voznesensky, Bin Bao, Peter Bell, David Berard, Evgeni Burovski, et al. Pytorch 2: Faster machine learning through dynamic python bytecode transformation and graph compilation. In *Proceedings of the 29th ACM International Conference on Architectural Support for Programming Languages and Operating Systems, Volume 2*, pages 929–947, 2024.
- Andrew Liu, Axel Elaldi, Nathan Russell, and Olivia Viessmann. Bio2token: All-atom tokenization of any biomolecular structure with mamba. *arXiv preprint arXiv:2410.19110*, 2024.
- Alec Radford, Jeffrey Wu, Rewon Child, David Luan, Dario Amodei, Ilya Sutskever, et al. Language models are unsupervised multitask learners. *OpenAI blog*, 1(8):9, 2019.
- Andrej Karpathy. karpathy/nanoGPT, January 2025. URL <https://github.com/karpathy/nanoGPT>. original-date: 2022-12-28T00:51:12Z.
- Aakanksha Chowdhery, Sharan Narang, Jacob Devlin, Maarten Bosma, Gaurav Mishra, Adam Roberts, Paul Barham, Hyung Won Chung, Charles Sutton, Sebastian Gehrmann, et al. Palm: Scaling language modeling with pathways. *Journal of Machine Learning Research*, 24(240):1–113, 2023.
- Mitchell Wortsman, Peter J Liu, Lechao Xiao, Katie Everett, Alex Alemi, Ben Adlam, John D Co-Reyes, Izzeddin Gur, Abhishek Kumar, Roman Novak, et al. Small-scale proxies for large-scale transformer training instabilities. *arXiv preprint arXiv:2309.14322*, 2023.
- Mario Michael Krell, Matej Kosec, Sergio P Perez, and Andrew Fitzgibbon. Efficient sequence packing without cross-contamination: Accelerating large language models without impacting performance. *arXiv preprint arXiv:2107.02027*, 2021.
- Ricky TQ Chen, Yulia Rubanova, Jesse Bettencourt, and David K Duvenaud. Neural ordinary differential equations. *Advances in neural information processing systems*, 31, 2018.
- Michael F Hutchinson. A stochastic estimator of the trace of the influence matrix for laplacian smoothing splines. *Communications in Statistics-Simulation and Computation*, 18(3):1059–1076, 1989.
- Raghunathan Ramakrishnan, Pavlo O Dral, Matthias Rupp, and O Anatole Von Lilienfeld. Quantum chemistry structures and properties of 134 kilo molecules. *Scientific data*, 1(1):1–7, 2014.
- Simon Axelrod and Rafael Gomez-Bombarelli. GEOM, energy-annotated molecular conformations for property prediction and molecular generation. *Scientific Data*, 9(1):1–14, 2022.
- Victor Garcia Satorras, Emiel Hoogeboom, and Max Welling. E (n) equivariant graph neural networks. In *International conference on machine learning*, pages 9323–9332. PMLR, 2021.
- Jiaming Song, Chenlin Meng, and Stefano Ermon. Denoising diffusion implicit models. *arXiv preprint arXiv:2010.02502*, 2020b.
- Cheng Lu, Yuhao Zhou, Fan Bao, Jianfei Chen, Chongxuan Li, and Jun Zhu. Dpm-solver: A fast ode solver for diffusion probabilistic model sampling in around 10 steps. *Advances in Neural Information Processing Systems*, 35: 5775–5787, 2022.
- Alex Morehead and Jianlin Cheng. Geometry-complete diffusion for 3d molecule generation and optimization. *Communications Chemistry*, 7(1):150, 2024.
- Peter Müller. Practical suggestions for better crystal structures. *Crystallography Reviews*, 15(1):57–83, 2009.
- Oleg V Dolomanov, Luc J Bourhis, Richard J Gildea, Judith AK Howard, and Horst Puschmann. Olex2: a complete structure solution, refinement and analysis program. *Journal of applied crystallography*, 42(2):339–341, 2009.
- Noel M O’Boyle, Michael Banck, Craig A James, Chris Morley, Tim Vandermeersch, and Geoffrey R Hutchison. Open babel: An open chemical toolbox. *Journal of cheminformatics*, 3:1–14, 2011.
- Patrick Kunzmann, Jacob Marcel Anter, and Kay Hamacher. Adding hydrogen atoms to molecular models via fragment superimposition. *Algorithms for Molecular Biology*, 17(1):7, 2022.
- Junjie Xie, Sheng Chen, Jinping Lei, and Yuedong Yang. Diffdec: structure-aware scaffold decoration with an end-to-end diffusion model. *Journal of Chemical Information and Modeling*, 64(7):2554–2564, 2024.

- Adi Haviv, Ori Ram, Ofir Press, Peter Izsak, and Omer Levy. Transformer language models without positional encodings still learn positional information. *arXiv preprint arXiv:2203.16634*, 2022.
- Amirhossein Kazemnejad, Inkit Padhi, Karthikeyan Natesan Ramamurthy, Payel Das, and Siva Reddy. The impact of positional encoding on length generalization in transformers. *Advances in Neural Information Processing Systems*, 36, 2024.
- Kulin Shah, Nishanth Dikkala, Xin Wang, and Rina Panigrahy. Causal language modeling can elicit search and reasoning capabilities on logic puzzles. *arXiv preprint arXiv:2409.10502*, 2024.
- Yann LeCun. Do large language models need sensory grounding for meaning and understanding. In *Workshop on Philosophy of Deep Learning, NYU Center for Mind, Brain, and Consciousness and the Columbia Center for Science and Society*, 2023.
- Gregor Bachmann and Vaishnavh Nagarajan. The pitfalls of next-token prediction. *arXiv preprint arXiv:2403.06963*, 2024.
- Jaeyeon Kim, Kulin Shah, Vasilis Kontonis, Sham Kakade, and Sitan Chen. Train for the worst, plan for the best: Understanding token ordering in masked diffusions. *arXiv preprint arXiv:2502.06768*, 2025.
- Jason Wei, Xuezhi Wang, Dale Schuurmans, Maarten Bosma, Fei Xia, Ed Chi, Quoc V Le, Denny Zhou, et al. Chain-of-thought prompting elicits reasoning in large language models. *Advances in neural information processing systems*, 35:24824–24837, 2022.
- Shibo Hao, Sainbayar Sukhbaatar, DiJia Su, Xian Li, Zhiting Hu, Jason Weston, and Yuandong Tian. Training large language models to reason in a continuous latent space. *arXiv preprint arXiv:2412.06769*, 2024.
- Frank Noé, Simon Olsson, Jonas Köhler, and Hao Wu. Boltzmann generators: Sampling equilibrium states of many-body systems with deep learning. *Science*, 365(6457):eaaw1147, 2019.
- Leon Klein, Andreas Krämer, and Frank Noé. Equivariant flow matching. *Advances in Neural Information Processing Systems*, 36:59886–59910, 2023.
- Leon Klein and Frank Noé. Transferable boltzmann generators. *arXiv preprint arXiv:2406.14426*, 2024.
- Charlie B Tan, Avishek Joey Bose, Chen Lin, Leon Klein, Michael M Bronstein, and Alexander Tong. Scalable equilibrium sampling with sequential boltzmann generators. *arXiv preprint arXiv:2502.18462*, 2025.
- Fabio Urbina, Filippa Lentzos, Cédric Invernizzi, and Sean Ekins. Dual use of artificial-intelligence-powered drug discovery. *Nature machine intelligence*, 4(3):189–191, 2022.
- Guido Van Rossum, Fred L Drake, et al. *Python reference manual*, volume 111. Centrum voor Wiskunde en Informatica Amsterdam, 1995.
- Travis E Oliphant. Python for scientific computing. *Computing in science & engineering*, 9(3):10–20, 2007.
- Adam Paszke, Sam Gross, Francisco Massa, Adam Lerer, James Bradbury, Gregory Chanan, Trevor Killeen, Zeming Lin, Natalia Gimelshein, Luca Antiga, et al. PyTorch: An imperative style, high-performance deep learning library. *Advances in Neural Information Processing Systems*, 32, 2019.
- William Falcon and The PyTorch Lightning team. PyTorch Lightning, March 2019. URL <https://github.com/Lightning-AI/lightning>.
- Greg Landrum, Paolo Tosco, Brian Kelley, Ric, David Cosgrove, sriniker, gedeck, Riccardo Vianello, NadineSchneider, Eisuke Kawashima, Dan N, Gareth Jones, Andrew Dalke, Brian Cole, Matt Swain, Samo Turk, AlexanderSavelyev, Alain Vaucher, Maciej Wójcikowski, Ichiru Take, Daniel Probst, Kazuya Ujihara, Vincent F. Scalfani, guillaume godin, Juuso Lehtivarjo, Rachel Walker, Axel Pahl, Francois Berenger, jasondbiggs, and strets123. rdkit/rdkit: 2023_03_3 (q1 2023) release, August 2023. URL <https://doi.org/10.5281/zenodo.8254217>.
- Nicholas Rego and David Koes. 3Dmol.js: Molecular visualization with WebGL. *Bioinformatics*, 31(8):1322–1324, 2015.
- Thomas Kluyver, Benjamin Ragan-Kelley, Fernando Pérez, Brian E Granger, Matthias Bussonnier, Jonathan Frederic, Kyle Kelley, Jessica B Hamrick, Jason Grout, Sylvain Corlay, et al. Jupyter notebooks—a publishing format for reproducible computational workflows. *Elpub*, 2016:87–90, 2016.
- John D Hunter. Matplotlib: A 2d graphics environment. *Computing in science & engineering*, 9(03):90–95, 2007.
- Michael L Waskom. Seaborn: statistical data visualization. *Journal of Open Source Software*, 6(60):3021, 2021.

- Charles R. Harris, K. Jarrod Millman, Stéfan J van der Walt, Ralf Gommers, Pauli Virtanen, David Cournapeau, Eric Wieser, Julian Taylor, Sebastian Berg, Nathaniel J. Smith, Robert Kern, Matti Picus, Stephan Hoyer, Marten H. van Kerkwijk, Matthew Brett, Allan Haldane, Jaime Fernández del Río, Mark Wiebe, Pearu Peterson, Pierre Gérard-Marchant, Kevin Sheppard, Tyler Reddy, Warren Weckesser, Hameer Abbasi, Christoph Gohlke, and Travis E. Oliphant. Array programming with NumPy. *Nature*, 585:357–362, 2020. doi: 10.1038/s41586-020-2649-2.
- Pauli Virtanen, Ralf Gommers, Travis E. Oliphant, Matt Haberland, Tyler Reddy, David Cournapeau, Evgeni Burovski, Pearu Peterson, Warren Weckesser, Jonathan Bright, Stéfan J. van der Walt, Matthew Brett, Joshua Wilson, K. Jarrod Millman, Nikolay Mayorov, Andrew R. J. Nelson, Eric Jones, Robert Kern, Eric Larson, C J Carey, İlhan Polat, Yu Feng, Eric W. Moore, Jake VanderPlas, Denis Laxalde, Josef Perktold, Robert Cimrman, Ian Henriksen, E. A. Quintero, Charles R. Harris, Anne M. Archibald, Antônio H. Ribeiro, Fabian Pedregosa, Paul van Mulbregt, and SciPy 1.0 Contributors. SciPy 1.0: Fundamental Algorithms for Scientific Computing in Python. *Nature Methods*, 17:261–272, 2020. doi: 10.1038/s41592-019-0686-2. URL <https://doi.org/10.1038/s41592-019-0686-2>.
- The pandas development team. pandas-dev/pandas: Pandas. URL <https://github.com/pandas-dev/pandas>.
- Juechu Dong, Boyuan Feng, Driss Guessous, Yanbo Liang, and Horace He. Flex attention: A programming model for generating optimized attention kernels. *arXiv preprint arXiv:2412.05496*, 2024.
- Ilya Loshchilov and Frank Hutter. Decoupled weight decay regularization. *arXiv preprint arXiv:1711.05101*, 2017.
- Tero Karras, Miika Aittala, Jaakko Lehtinen, Janne Hellsten, Timo Aila, and Samuli Laine. Analyzing and improving the training dynamics of diffusion models. In *Proceedings of the IEEE/CVF Conference on Computer Vision and Pattern Recognition*, pages 24174–24184, 2024.
- Yeonjoon Kim and Woo Youn Kim. Universal structure conversion method for organic molecules: from atomic connectivity to three-dimensional geometry. *Bulletin of the Korean Chemical Society*, 36(7):1769–1777, 2015.

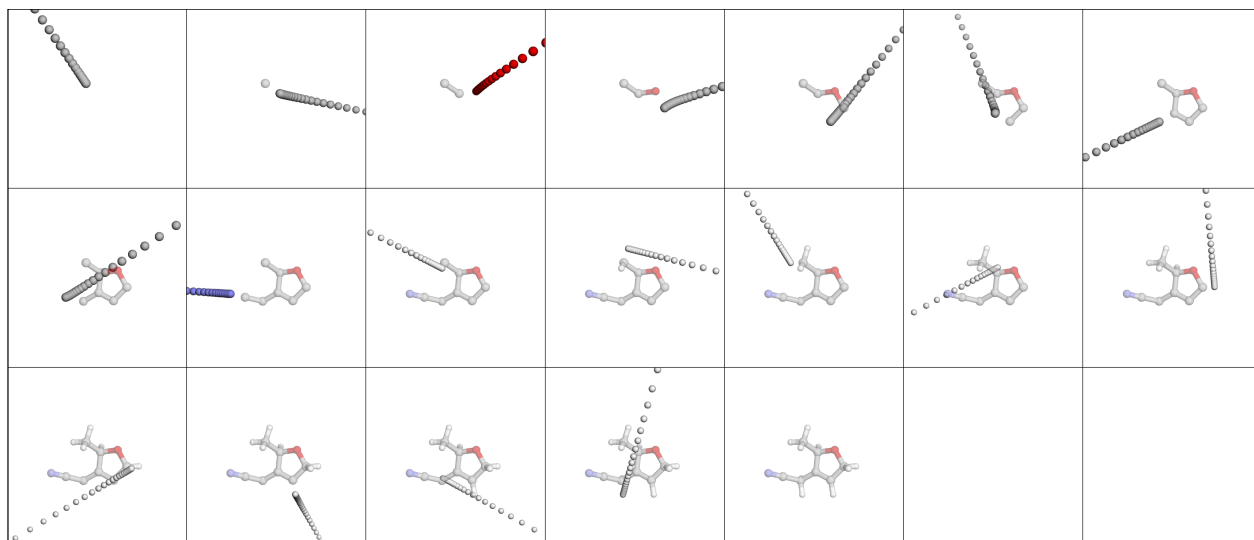


Figure 5 QUETZAL generates 3D molecules by iteratively predicting the next atom’s discrete type and continuous 3D position. The continuous trajectories of the DiffMLP are shown at every step.

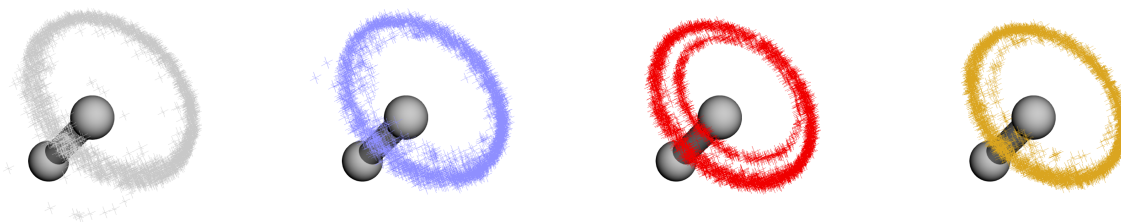


Figure 6 Next position distributions for carbon, nitrogen, oxygen, and fluorine. The model learns to make symmetric predictions from data augmentation.

A Karras et al. (2022) diffusion framework

Following the framework of Karras et al. (2022), we precondition the neural network using the following reparameterization,

$$D_{\theta}(t, \mathbf{x}^{\text{noisy}}) = \frac{\sigma_{\text{data}}^2}{t^2 + \sigma_{\text{data}}^2} \mathbf{x}^{\text{noisy}} + \frac{t\sigma_{\text{data}}}{\sqrt{t^2 + \sigma_{\text{data}}^2}} F_{\theta} \left(\frac{\mathbf{x}^{\text{noisy}}}{\sqrt{t^2 + \sigma_{\text{data}}^2}}, \frac{1}{4} \ln t \right), \quad (12)$$

where σ_{data} is a hyperparameter set to the standard deviation of the coordinates depending on the dataset, and F_{θ} is the actual DiffMLP.

During training, timesteps are sampled from a log-normal distribution $\ln t \sim \mathcal{N}(-1.2, 1.2^2)$, and the denoising score matching loss of Equation (9) on each timestep is weighted by $(t^2 + \sigma_{\text{data}}^2)/(t\sigma_{\text{data}})^2$. For sampling, we use the Heun integrator, which evaluates D_{θ} twice per integration timestep, and the discretized timesteps are geometrically spaced, given by

$$t_i = \left(\sigma_{\text{max}}^{1/\rho} + \frac{i}{N_{\text{diff}} - 1} (\sigma_{\text{min}}^{1/\rho} - \sigma_{\text{max}}^{1/\rho}) \right)^{\rho}, \quad (13)$$

where N_{diff} is the number of diffusion steps, $\rho = 7$, $\sigma_{\text{min}} = 10^{-4}$, and $\sigma_{\text{max}} = 80$.

B Experimental details

We use the same train/val/test splits as [Hoogeboom et al. \(2022\)](#), which contain 10,000/17,748/13,083 examples for QM9 and 5,538,014/692,251/692,251 examples for GEOM.

We train models on QM9 for 2000 epochs. We use sequence packing, using the Longest-pack-first histogram-packing algorithm ([Krell et al., 2021](#)). Before training, we pack all examples into sequences of size 128, enforcing a maximum of 6 examples per pack. We then batch packs together by concatenating across the length dimension, with a batch size of 180 packs. This procedure of batching packs was necessary for keeping uniform the number of examples per pack, which was vital for efficient and stable training convergence. We train for 2000 epochs (188k steps) on a single A100 40GB GPU, which took a wall-time of 21 hours. We do document masking using FlexAttention ([Dong et al., 2024](#)), preventing the model from attending to other examples in the batched pack.

We do gradient clipping to a norm of 1.0. We train with AdamW ([Loshchilov and Hutter, 2017](#)) using a learning rate of 4×10^{-4} , $\beta_1 = 0.9$, $\beta_2 = 0.95$, and weight decay = 10^{-5} . We maintain an exponential moving average of the parameters with decay rate 0.999. We use $\sigma_{\text{data}} = 1.4$ for QM9, and $\sigma_{\text{data}} = 2.5$ for GEOM.

Fourier encodings were important for efficient learning and are used in three different parts of the architecture:

1. For embedding coordinates in the transformer, each element of a vector of size 3 is mapped to 256 Fourier channels with bandwidth $b = 20$, before flattening to size 768.
2. For embedding coordinates in the DiffMLP, each element of each vector of size 3 is mapped to 512 Fourier channels with bandwidth $b = 20$, before flattening to size 1536.
3. For embedding timestep in the DiffMLP, a scalar is mapped to w Fourier channels with bandwidth $b = 1$, where w is the width of the DiffMLP.

We use the magnitude-preserving Fourier encodings proposed by [Karras et al. \(2024\)](#). A scalar x is mapped to a vector of Fourier features via $x \mapsto \sqrt{2} \cos(2\pi(bf_i x + \varphi_i))$, where b is the bandwidth, and frequencies $f_i \sim \mathcal{N}(0, 1)$ and phases $\varphi_i \sim \mathcal{U}[0, 1]$ are randomly initialized constants.

For GEOM, we train with 4 A100 40GB GPUs for 201 epochs (734k steps). We use a learning rate of 2×10^{-4} per GPU. We pack all examples into sequences of size 512, enforcing a maximum of 10 examples per pack, and use a batch size of 40 packs per batch.

B.1 Metrics

[Garcia Satorras et al. \(2021\)](#) introduce several metrics for evaluating the quality of generated 3D molecules. They define a lookup table of allowed bond lengths, with thresholds tuned to maximize the validity of each dataset. A molecule is assigned bonds using this lookup table, and then the valency of each atom is checked. An atom is stable if it has the correct valency. A molecule is stable if all of its atoms are stable. Atom stability is the proportion of generated atoms which are stable. Molecule stability is the proportion of generated molecules which are stable. A molecule is valid if its assigned bonds can be parsed by RDKit without failure. Validity is the proportion of generated examples which are valid. If the molecule can be parsed by RDKit, then it can be turned into a SMILES string. Uniqueness is calculated as the number of unique, generated SMILES strings divided by the number of generated molecules.

We use RDKit’s xyz2mol ([Kim and Kim, 2015](#)), specifically we use rdkit==2023.03.3 with rdDetermineBonds.DetermineBonds(mol, charge=0). A molecule is valid if this function passes without error and the resulting molecule can be turned into a SMILES string. We found that this version of RDKit reproduces the results of ([Daigavane et al., 2023](#)), and determines 99.99% of the QM9 training set to be valid, whereas later versions of RDKit only determines 94.78% to be valid.

We estimate the first row of [Table 2](#) by computing metrics for 200k random examples from the training set of GEOM.

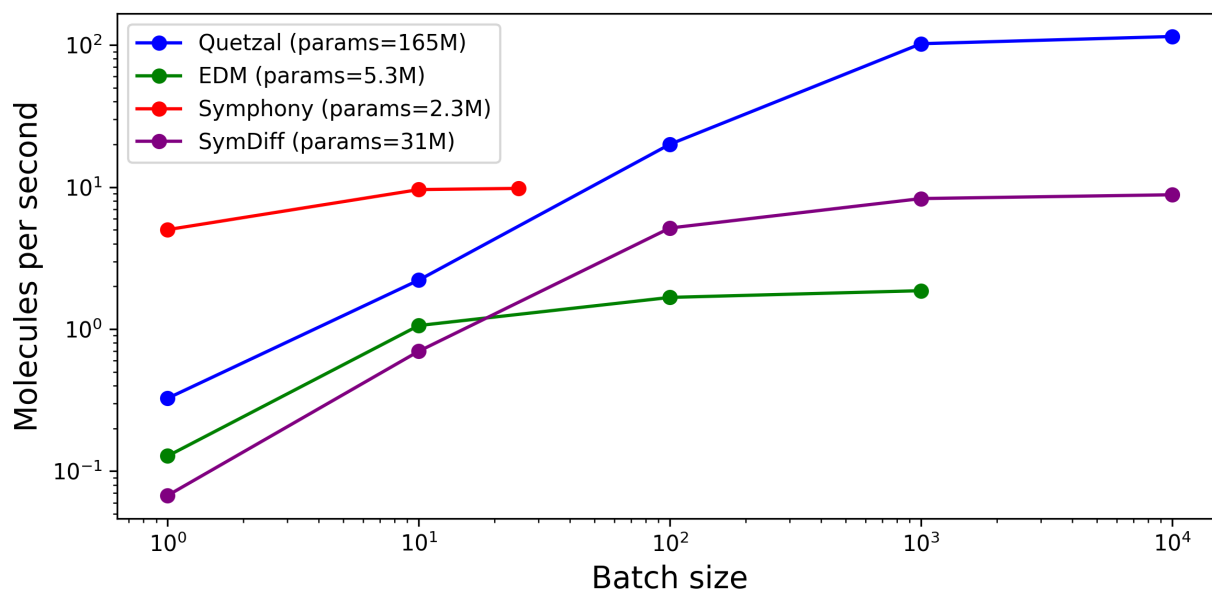


Figure 7 Generation speed of QM9 examples as a function of batch size on a single A100 40GB GPU. Despite having over 5× as many parameters as baselines, QUETZAL scales to large batch sizes at inference time, enabling fast amortized generation.

B.2 Architecture ablation

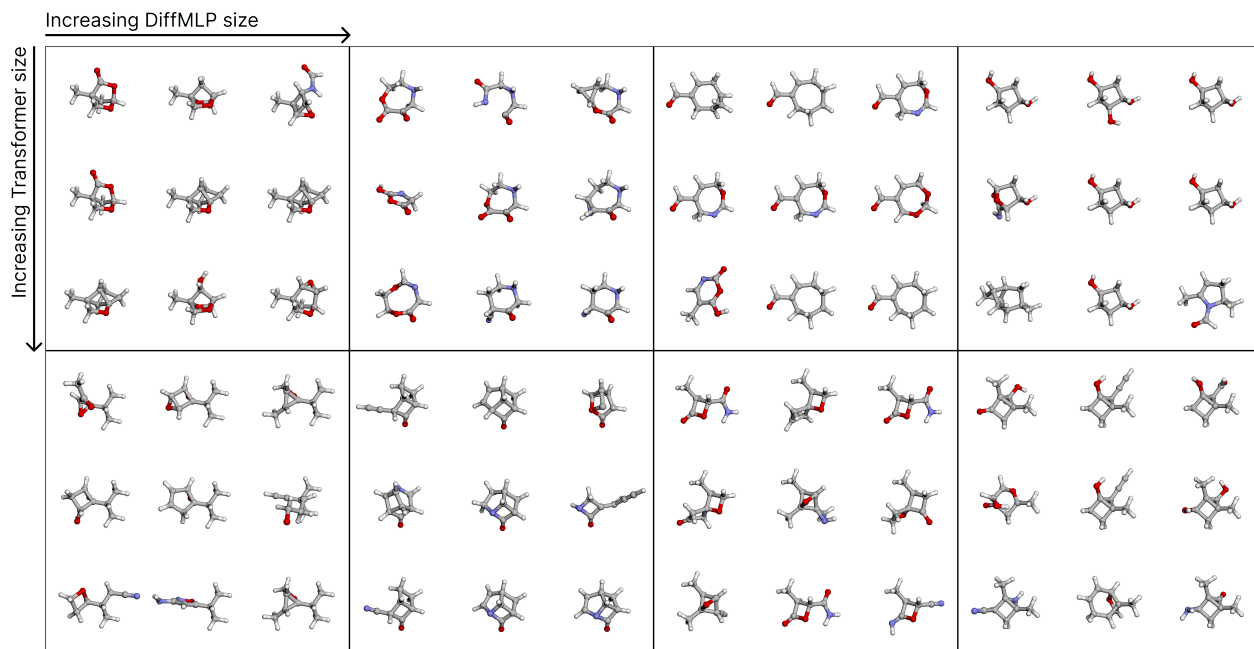


Figure 8 Generated samples using the same random generation seed for different sized models. $N_{\text{diff}} = 30$ diffusion steps are used for each atom. Different models converge to similar molecules. Both the transformer and DiffMPL are important in controlling structure. Model sizes in [Table 4](#).

Table 4 Ablation of transformer and DiffMPL size. W is the transformer width, H is the number of heads, and L is the number of layers. w is the DiffMPL width. Results show mean and standard deviation across 3 evaluation runs.

Transformer size	MLP width	atom stable	mol stable	lookup valid	lookup valid×uniq	xyz2mol valid	xyz2mol valid×uniq
$W = 512$	$w = 512$	96.0±0.1	73.8±0.4	87.5±0.2	84.4±0.2	95.8±0.1	91.6±0.2
$H = 8$	$w = 1024$	97.4±0.1	81.6±0.5	91.6±0.2	88.1±0.3	98.2±0.1	94.0±0.3
$L = 8$	$w = 1536$	97.7±0.0	83.4±0.2	92.6±0.2	88.9±0.1	98.4±0.1	94.0±0.0
$W = 640$	$w = 512$	97.1±0.1	80.6±0.4	91.1±0.4	87.3±0.5	96.8±0.2	92.2±0.2
$H = 10$	$w = 1024$	97.6±0.0	82.9±0.3	92.5±0.1	88.7±0.1	98.4±0.1	93.9±0.2
$L = 10$	$w = 1536$	98.0±0.1	85.7±0.6	93.8±0.4	89.8±0.4	98.9±0.1	94.0±0.2
$W = 768$	$w = 512$	96.7±0.1	78.6±0.4	90.3±0.1	85.9±0.1	97.1±0.0	91.7±0.2
$H = 12$	$w = 1024$	97.9±0.0	85.8±0.2	93.6±0.2	89.3±0.2	98.4±0.1	93.5±0.3
$L = 12$	$w = 1536$	98.3±0.0	87.6±0.3	94.7±0.2	90.1±0.1	99.1±0.0	94.0±0.1
with atom permutations		82.3±0.1	25.9±0.2	63.1±0.5	62.5±0.4	80.7±0.2	80.1±0.3
w/o translations & rotations		98.2±0.0	86.6±0.3	94.1±0.2	89.5±0.3	98.8±0.1	93.6±0.1

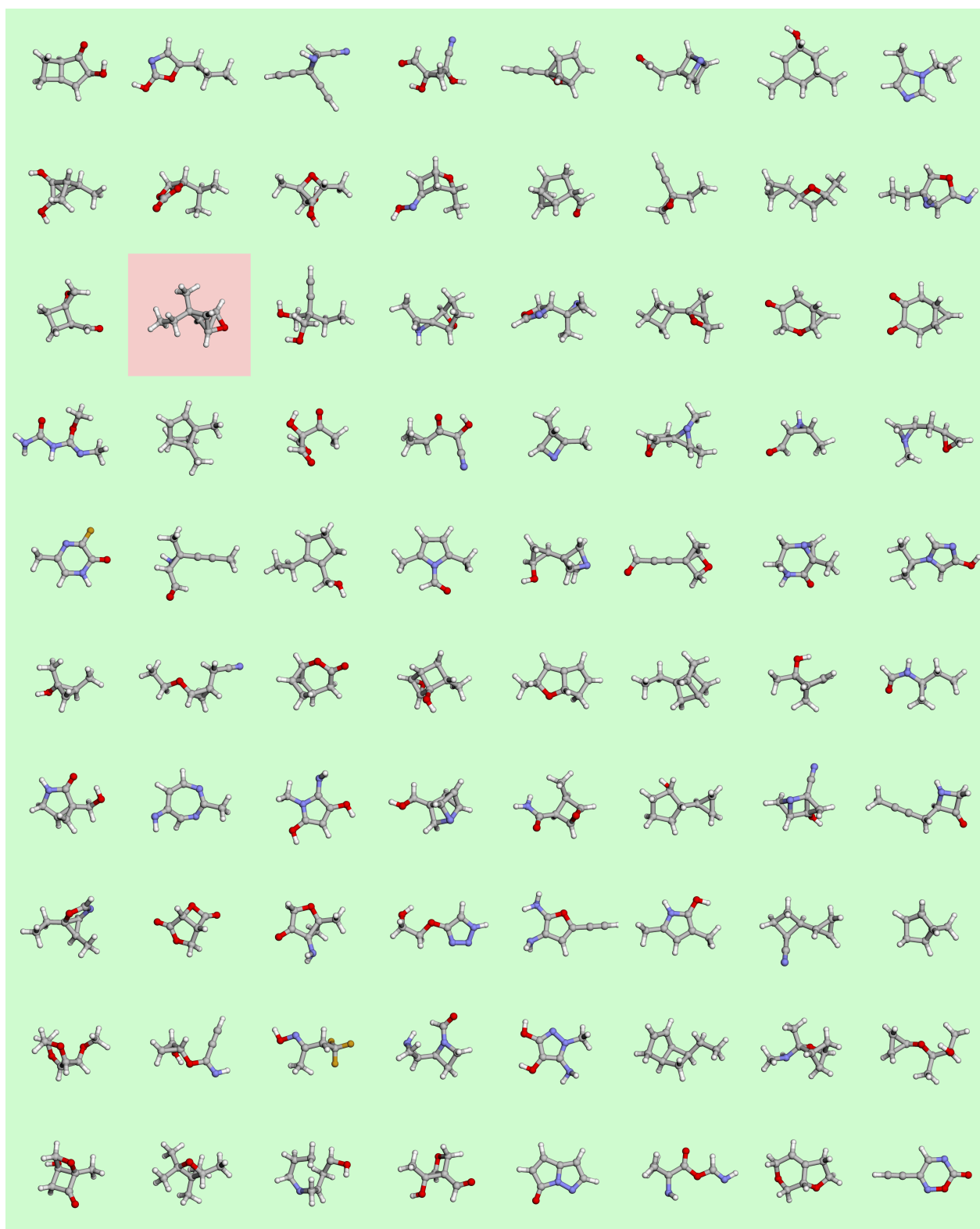


Figure 9 Uncurated generated molecules from QM9. Green/red indicates valid/invalid by xyz2mol.



Figure 10 Uncurated generated molecules from GEOM. Green/red indicates valid/invalid by xyz2mol.

B.3 Hydrogen decoration

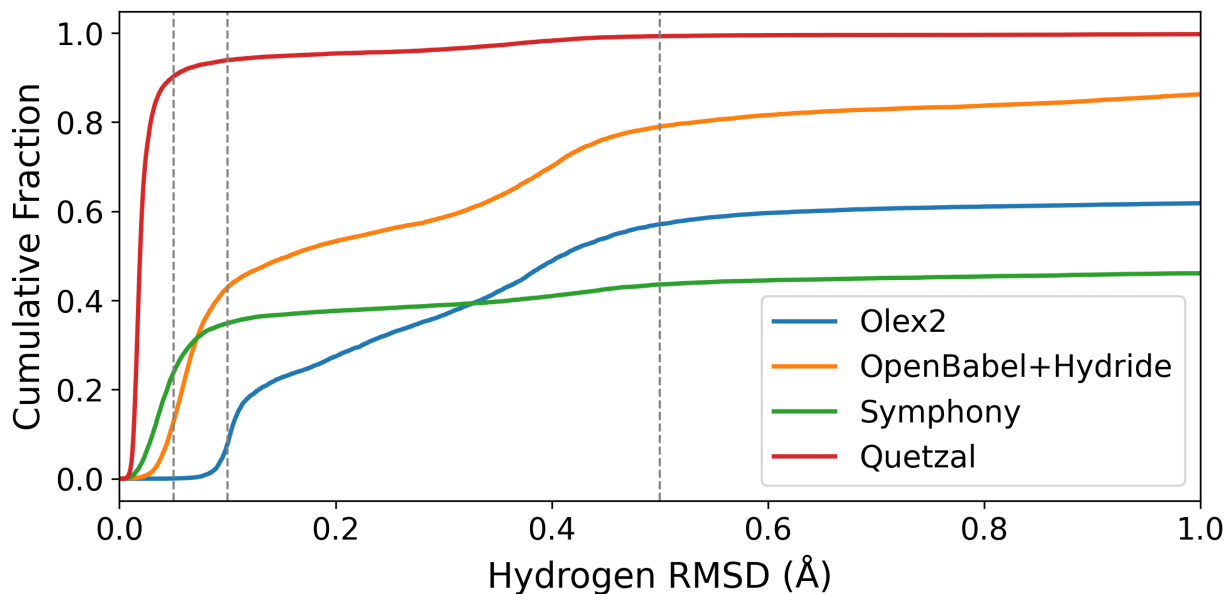


Figure 11 Cumulative distribution functions of RMSD after decorating bare molecules from the test set of QM9. QUETZAL adds hydrogens with very low RMSD for a large majority of the test set. Adding an incorrect number of hydrogens is treated as $\text{RMSD} = \infty$. The vertical dotted lines are the thresholds 0.5, 0.1, 0.05 Å as shown in Table 3. The checkpoint for Symphony appears to be undertrained: https://github.com/atomicarchitects/symphony/blob/3f2c6a7f7983877f4a5f2a0a71328b29bdc553cf/tutorial/workdir/checkpoints/params_best.pkl

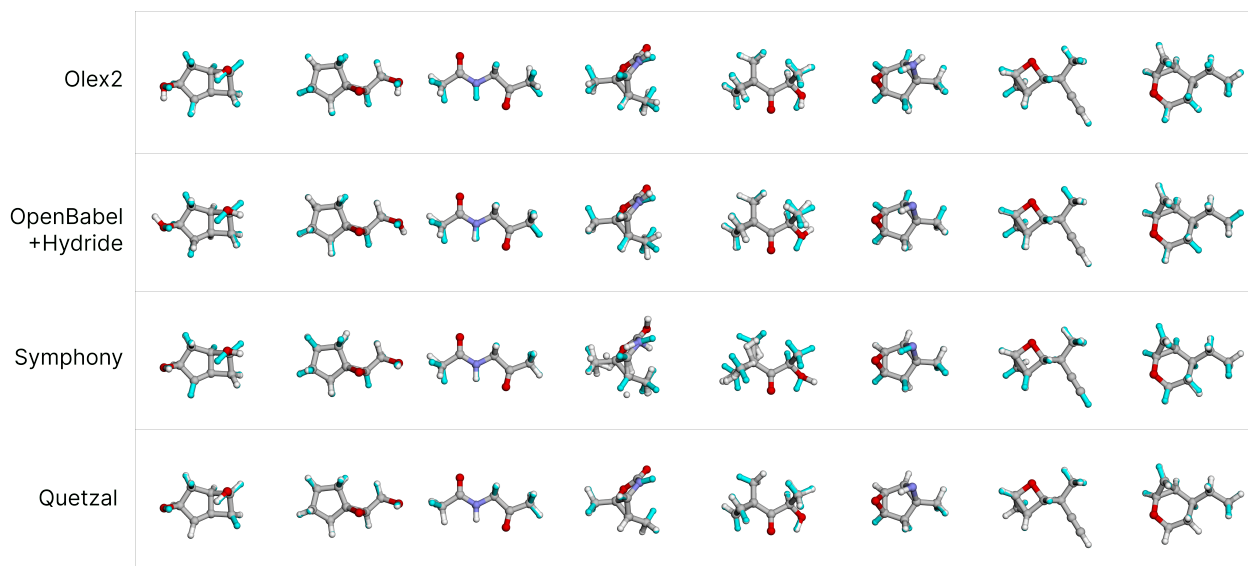


Figure 12 Comparison of methods for adding hydrogens in 3D. The ground truth is displayed in cyan. Accurate hydrogen placement for hydroxyl and methyl groups is difficult.

C Licenses

Datasets:

- QM9 ([Ramakrishnan et al., 2014](#)): The license status is unclear
- GEOM ([Axelrod and Gomez-Bombarelli, 2022](#)): CC0 1.0 Universal

Models:

- EDM ([Hoogeboom et al., 2022](#)): MIT License
- Symphony ([Daigavane et al., 2023](#)): MIT License
- SymDiff ([Zhang et al., 2024](#)): MIT License